◆ Human Brain Mapping 35:5262–5278 (2014) ◆

Atomic Dynamic Functional Interaction Patterns for Characterization of ADHD

Jinli Ou,[1] Zhichao Lian,[2] Li Xie,[1] Xiang Li,[3] Peng Wang,[4] Yun Hao,[5] Dajiang Zhu,[3] Rongxin Jiang,[1] Yufeng Wang,[4] Yaowu Chen,[1] Jing Zhang,[2]* and Tianming Liu[3]*

[1]*School of Biomedical Engineering & Instrument Science, Zhejiang University, Hangzhou, China*
[2]*Department of Statistics, Yale University, New Haven, CT*
[3]*Cortical Architecture Imaging and Discovery Lab, Department of Computer Science and Bioimaging Research Center, The University of Georgia, Athens, Georgia*
[4]*Institute of Mental Health, Peking University, Beijing, China*
[5]*School of Life Sciences, Fudan University, Shanghai, China*

Abstract: Modeling abnormal temporal dynamics of functional interactions in psychiatric disorders has been of great interest in the neuroimaging field, and thus a variety of methods have been proposed so far. However, the temporal dynamics and disease-related abnormalities of functional interactions within specific data-driven discovered subnetworks have been rarely explored yet. In this work, we propose a novel computational framework composed of an effective Bayesian connectivity change point model for modeling functional brain interactions and their dynamics simultaneously and an effective variant of nonnegative matrix factorization for assessing the functional interaction abnormalities within subnetworks. This framework has been applied on the resting state fmagnetic resonance imaging (fMRI) datasets of 23 children with attention-deficit/hyperactivity disorder (ADHD) and 45 normal control (NC) children, and has revealed two atomic functional interaction patterns (AFIPs) discovered for ADHD and another two AFIPs derived for NC. Together, these four AFIPs could be grouped into two pairs, one common pair representing the common AFIPs in ADHD and NC, and the other abnormal pair representing the abnormal AFIPs in ADHD. Interestingly, by comparing the abnormal AFIP pair, two data-driven abnormal functional subnetworks are derived. Strikingly, by evaluating the approximation based on the four AFIPs, all of the ADHD children were successfully differentiated from NCs without any false positive. *Hum Brain Mapp 35:5262–5278, 2014.* © 2014 Wiley Periodicals, Inc.

Key words: brain networks; functional interaction; temporal dynamics; nonnegative matrix factorization; ADHD

Additional Supporting Information may be found in the online version of this article.

Contract grant sponsor: NIH (T.L); Contract grant number: R01 DA-033393; Contract grant sponsor: NIH (T.L); Contract grant number: R01 AG-042599; Contract grant sponsor: NSF CAREER Award (T.L); Contract grant number: IIS-1149260; Contract grant sponsor: NSF (T.L); Contract grant number: CBET-1302089; Contract grant sponsor: Start-up funding and Sesseel Award from Yale University (J.Z).

*Correspondence to: J. Zhang, Department of Statistics, Yale University, Connecticut. E-mail: jing.maria.zhang@gmail.com or T. Liu, Department of Computer Science and Bioimaging Research Center, The University of Georgia, Athens, GA. E-mail: tianming.liu@gmail.com

Received for publication 8 December 2013; Revised 7 March 2014; Accepted 5 May 2014.
Jinli Ou and Zhichao Lian are Joint first authors.
DOI: 10.1002/hbm.22548
Published online 23 May 2014 in Wiley Online Library (wileyonlinelibrary.com).

INTRODUCTION

Recently, modeling functional connectivity between anatomically distinct regions of interest (ROIs) in the brain has emerged as a powerful tool for investigating functional brain interactions and their abnormalities in psychiatric conditions. In many previous functional connectivity studies [Fox and Raichle, 2007; Raichle et al., 2001], functional connectivities or interactions were assumed to be temporally stationary, that is, functional connectivities or interactions were estimated over the entire fMRI scan. However, recent studies suggested that the functional activity/connectivity of any cortical area is subject to top-down influences of attention, expectation, and perceptual tasks [Gilbert and Sigman, 2007]. For example, each brain area performs quite different programs according to the context and to the current perceptual requirements [Gilbert and Sigman, 2007]. Particularly, the dynamically changing functional interactions from higher- to lower-order brain areas and intrinsic cortical networks mediate the moment-by-moment functional state changes in the brain [Gilbert and Sigman, 2007; Li et al., 2013a]. Even in resting state, a variety of studies have suggested that the functional interaction is still undergoing considerable temporal dynamic changes at different time scales [e.g., Bassett et al., 2011; Chang and Glover, 2010; Li et al., 2013a, 2014b; Lindquist et al., 2007; Lynall et al., 2010; Majeed et al., 2011; Robinson et al., 2010; Smith et al., 2012; Zhang et al., 2012].

Along this research direction, there are several recent literature reports that used sliding time windows to capture the functional brain dynamics [e.g., Allen et al., 2012; Li et al., 2013a; Zhang et al., 2012]. However, the effectiveness of the sliding time window based framework might be limited due to the difficulty in determining the optimal length of the sliding time window and its biological meaning. Considering the temporal state-like and network behaviors of functional brain interactions, we utilize our recently developed Bayesian connectivity change point mode (BCCPM) [Lian et al., In press; Zhang et al., 2013a] to statistically investigate the temporal dynamics of functional interactions, which can be characterized by large-scale functional connectivity matrices, for example, denoted by $\mathbf{V}$. Then, from a mathematical perspective, any given matrix $\mathbf{V}$ can be approximated by a linear combination of some orthogonal bases [Trefethen and Bau III, 1997], for example, $\mathbf{V} \approx \mathbf{WH}$. Under the nonnegative constraint, the nonnegative matrix factorization (NMF) can effectively learn the orthogonal bases [e.g., Lee and Seung, 1999; Yang et al., 2007]. Essentially, each entry of columns of the coefficient matrix $\mathbf{H}$ indicates the contribution of each basis to the approximation of samples $\mathbf{V}$. By considering each basis, that is, each column of $\mathbf{W}$, as a distinctive cluster, and choosing the maximum of each column of coefficient matrix as the cluster indicator, NMF can effectively learn the bases and the clustering results simultaneously [e.g., Brunet et al., 2004; Ding et al., 2005; Li and Ding, 2006; Yang et al., 2007]. Recently, NMF and its variants have been successfully applied to biomedical scenarios [Brunet et al., 2004; Ghanbari et al., 2013; Kim and Park, 2007; Pascual-Montano et al., 2006; Qi et al., 2009].

From a technical perspective, it is difficult to integrate and compare the fMRI signals and their derivations across different brains without a generic brain reference system. Because of the unclear cortical boundaries, the remarkable individual structural variability of cortical anatomy and the nonlinear properties of ROIs [Liu, 2011], identifying a common and reliable set of brain landmarks across different brains as a generic reference system is perhaps one of the great challenges in human brain mapping [Derrfuss and Mar, 2009; Poldrack, 2012]. Recently, a large set of common and consistent cortical landmarks has been developed and publicly released, named Dense Individualized and Common Connectivity-based Cortical Landmarks (DICCCOL) [Zhu et al., 2013]. The neuroscience basis is the "connectional fingerprint," that is, each cytoarchitectonic area possesses a unique set of extrinsic inputs and outputs, which is crucial in the determination of the functions that the area can perform [Passingham et al., 2002]. In current stage, the DICCCOL approach has discovered 358 common and consistent cortical ROIs, each of which is optimized to possess maximal group-wise consistency of diffusion tensor imaging (DTI)-derived fiber shape patterns [Zhu et al., 2013]. Importantly, the set of the 358 DICCCOL landmarks can be accurately predicted and localized in the DTI data of an individual brain. Due to intrinsically established structural and functional correspondences of the DICCCOLs across different individuals and populations, they offer a generic brain reference system for integrating and comparing fMRI data across individuals and populations. Thus, in this work, we adopted the 358 DICCCOL landmarks as network nodes for functional interaction pattern (FIP) mapping.

In addition, motivated by the temporal dynamics of functional interactions [Bassett et al., 2011; Chang and Glover, 2010; Majeed et al., 2011; Smith et al., 2012] and inspired by the success of projective nonnegative matrix factorization based on the Frobenius norm (NPNMF) in learning connectivity subnetworks [Ghanbari et al., 2013], we propose a novel computational framework that combines the effective BCCPM and the projective nonnegative matrix factorization based on a variant of Kullback–Leibler divergence (DPNMF), to infer temporal dynamics of functional interactions and learn the FIPs within subnetworks, which are called atomic functional interaction patterns (AFIPs). Specifically, a key concept in the BCCPM is that change points are defined as abrupt changes of multivariate functional interactions among brain networks, other than the raw fMRI time series changes [e.g., Lindquist et al., 2007; Robinson et al., 2010]. In both DPNMF and NPNMF, $\mathbf{H}$ is assumed to be the projection of $\mathbf{V}$ to $\mathbf{W}$. Hence we only need to update $\mathbf{W}$ during matrix factorization, while both $\mathbf{W}$ and $\mathbf{H}$ need to be updated in the standard nonnegative matrix factorization (SNMF) [Brunet et al., 2004; Lee and Seung, 1999]. The major difference between DPNMF and NPNMF is that the

objective function in DPNMF is based on the matrix divergence, which can be reduced to the Kullback–Leibler divergence, other than the matrix norm. The DPNMF approach can converge more quickly and achieve more stable clustering results, as compared with SNMF and NPNMF and discussed in the following sections.

The applicability of the computational framework has been demonstrated by applying it to the multimodal DTI and resting state fMRI (R-fMRI) datasets of 23 attention-deficit/hyperactivity disorder (ADHD) children and 45 normal control (NC) ones. Experimental results have suggested two AFIPs discovered for ADHD and the other two AFIPs derived for NC. Importantly, these four AFIPs could be categorized into two pairs, one common pair representing the common AFIPs in ADHD and NC, and the other abnormal pair representing the abnormal AFIPs in ADHD. By comparing the abnormal AFIP pair, two data-driven abnormal functional subnetworks (AFSNs) were derived. Interestingly, by evaluating the approximation based on the four AFIPs, all of the ADHD children were successfully differentiated from the NC ones without any false positive. In general, our work contributed a novel computational framework for dynamic functional interaction modeling and our experimental results demonstrated that the atomic dynamic FIPs offer meaningful neuroscientific insights and can effectively characterize and differentiate ADHD children from NC ones.

MATERIALS AND METHODS

Overview

The flowchart of the proposed computational framework is summarized in Figure 1. First, the 358 consistent DICCCOL landmarks that have been discovered and validated in our recent study [Zhu et al., 2013] are predicted and localized in the DTI data of each brain (green bubbles in Fig. 1a) via a data-driven strategy [Zhu et al., 2012, 2013]. After DICCCOL prediction, the R-fMRI images are coregistered into the DTI space using FMRIB software library (FSL) FMRIB's linear image registration tool (FLIRT), and then the R-fMRI time series corresponding to each DICCCOL are extracted. Subsequently, change points in the extracted R-fMRI time series of each subject are modeled and detected via the BCCPM (Fig. 1b). Then FIPs were estimated (Fig. 1c) as the Pearson correlations between every pair of the R-fMRI time series segments separated by those change points and then vectorized to construct a vector, named functional connectome vector (FCV). Due to the intrinsic structural and functional correspondences of DICCCOLs across different individuals and populations, FCVs derived from different R-fMRI time series segments across different brains were integrated and pooled to form a single FCV matrix (Fig. 1d). Finally, we perform the atomic functional interaction pattern learning (AFIPL) using the DPNMF [Yang and Oja, 2010] (Fig. 1e). Details of these steps will be described in details in the following sections.

Data Acquisition and Preprocessing

The DTI and R-fMRI datasets used in this work were acquired from 74 children including 25 ADHD-c (a subtype of ADHD which exhibits both inattention and hyperactivity-impulsivity symptoms) patients and 49 normal development children as NCs under Institutional Review Board (IRB) approval. These participants were all aged between 8 and 14 years and right-handed, and their intelligence quotient were higher than 80. All the children were diagnosed by the Kiddie Schedule for Affective Disorders and Schizophrenia for School-Age Children-Present and Lifetime Version (K-SADS-PL)[Kaufman et al., 1997], and they agreed to participant in this study, from whose parents' informed consent was obtained. Due to excessive head motion during R-fMRI scans, two patients and four NCs were excluded. Totally, we had 23 ADHD patients and 45 NCs involved in this study.

The datasets were acquired with a 3T Siemens Trio scanner at the Imaging Center for Brain Research, Beijing Normal University, with the following parameters. R-fMRI: axial slices, 33; repetition time (TR), 2000 ms; echo time (TE), 30 ms; flip angle (FA), 90; thickness/gap, 3.5/0.7 mm; field of view (FOV), 200 × 200 mm^2; matrix, 64 × 64. DTI: axial slices, 49; TR, 7200 ms; TE, 104 ms; diffusion directions, 64; b, 1000 s/mm^2; average, 1; thickness, 2.5 mm; acquisition matrix, 128 × 128; FOV, 230 × 230 mm^2.

Bayesian Connectivity Change Point Model

As mentioned above, we know that the FIP is undergoing temporal dynamic changes. Motivated by the state-like behavior of functional interactions, our recently developed novel Bayesian connectivity change point model (BCCPM) [Lian et al., In press; Zhang et al., 2013a] is applied to the R-fMRI time series for detecting the change points, which are defined as abrupt changes of multivariate functional interactions among brain networks. To be self-contained and be brief, in the BCCPM, the change points are determined by the joint probability among ROIs between different time periods, and Markov chain Monte Carlo (MCMC) is applied to sample the posterior probability distribution of each time point as being a change point. Let $\mathbf{X}^s = [x_1^s, x_2^s, \cdots, x_M^s]$, $x_t^s \in \mathcal{R}^m$ be the R-fMRI time series of a subject s, where m is the number of ROIs, M is the total number of time points per subject, the superscript s denotes subject index, which will be omitted if we do not refer to any specific subject, and the subscript t denotes time index. We assume the R-fMRI time series to be a Gaussian distribution, that is, $x_t \sim N(\mu, \Sigma)$, where μ denotes the m-dimensional mean vector, and $\sum$ denotes the $m \times m$ covariance matrix. The conjugate prior

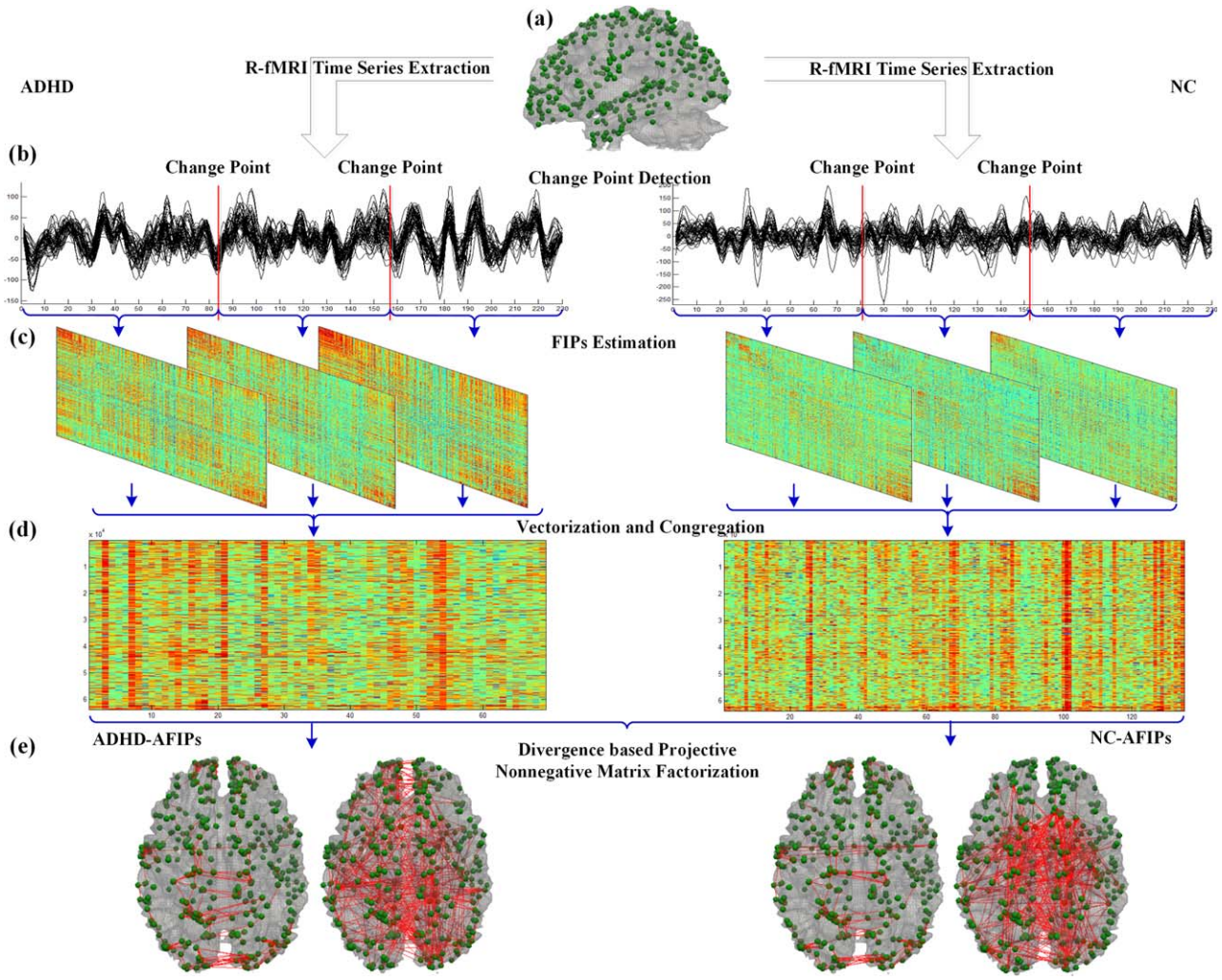

Figure 1.

The flowchart of the computational framework. (**a**) The 358 DICCCOLs prediction and R-fMRI time series extraction for each DICCCOL. (**b**) Change points detection in the R-fMRI time series of each subject via the BCCPM. (**c**) FIP estimation as the Pearson correlation between every pair of the R-fMRI time series segments separated by those detected change points. (**d**) FIP matrix vectorization and congregation. (**e**) AFIPL via the *DPNMF approach*. [Color figure can be viewed in the online issue, which is available at wileyonlinelibrary.com.]

distribution of (μ, Σ) is the $N-\text{Inv}-\text{Wishart}\,(\mu_0, \Lambda_0/\kappa_0, \nu_0, \Lambda_0)$ [Gelman et al., 2003] with the following form:

$$\mu|\Sigma \sim N(\mu_0, \Sigma/\kappa_0), \quad \Sigma \sim \text{Inv}-\text{Wishart}\,(\nu_0, \Lambda_0). \tag{1}$$

Based on the data $x_1, x_2, \cdots, x_M$, the posterior distribution of $(\mu, \sum)$ is $N-\text{Inv}-\text{Wishart}\,(\mu_M, \Lambda_M/\kappa_M, \nu_M, \Lambda_M)$, where

$$\mu_M = \frac{\kappa_0}{\kappa_0+M}\mu_0 + \frac{M}{\kappa_0+M}\bar{x}, \quad \kappa_M = \kappa_0+M, \quad \nu_M = \nu_0+M$$

$$\Lambda_M = \Lambda_0 + S + \frac{\kappa_0 M}{\kappa_0+M}(\bar{x}-\mu_0)(\bar{x}-\mu_0)^T, \quad S = \sum_{t=1}^{M}(x_t-\bar{x})(x_t-\bar{x})^T. \tag{2}$$

Therefore, the probability of $x_1, x_2, \cdots, x_M$ is calculated as follows [Gelman et al., 2003]:

$$\begin{aligned} p(x_1, x_2, \cdots, x_M) &= \frac{p(x_1, x_2, \cdots, x_M; \mu, \Sigma)}{p(\mu, \Sigma|x_1, x_2, \cdots, x_M)} \\ &= \left(\frac{1}{2\pi}\right)^{mM/2} \times 2^{mM/2} \times \left(\frac{\kappa_0}{\kappa_M}\right)^{m/2} \\ &\times \frac{\Gamma_m(\frac{\nu_M}{2})(\det(\Lambda_0))^{\nu_0/2}}{\Gamma_m(\frac{\nu_0}{2})(\det(\Lambda_M))^{\nu_M/2}}, \end{aligned} \tag{3}$$

where Γ_m is the multivariate gamma function:

$$\Gamma_m(x)=\pi^{m(m-1)/2}\prod_{j=1}^{m}\Gamma(x+(1-j)/2)\ . \quad (4)$$

Then we define a segment indicator vector $\overrightarrow{I}=(I_1,I_2,\ldots,I_M)$ to indicate the possible locations of the change points in the $m \times M$ R-fMRI time series matrix $\mathbf{X}=[x_1,x_2,\ldots,x_M]$, where $I_t=1$ indicates that there is a change point at time Point t, $I_t=0$ otherwise. The starting time point I_1 is always considered as a change point, as it is the beginning of the first segment. Given $\overrightarrow{I}$, the marginal likelihood of the R-fMRI time series matrix $\mathbf{X}=[x_1,x_2,\ldots,x_M]$ can be represented as follows:

$$p\left(\mathbf{X}|\overrightarrow{I}\right)=\prod_{b=1}^{\sum I_t}p(\mathbf{X}_b)\ , \quad (5)$$

where $\mathbf{X_b}$ is the temporal samples belonging to the b-th segment and $p(\mathbf{X_b})$ can be calculated according to Eq. (3). It should be pointed out that the temporal segments are assumed to be statistical independent here. Therefore, the posterior distribution of $p(\overrightarrow{I}|\mathbf{X})$ can be obtained by:

$$p\left(\overrightarrow{I}|\mathbf{X}\right)\propto p\left(\overrightarrow{I}\right)p\left(\mathbf{X}|\overrightarrow{I}\right)\ , \quad (6)$$

where $p\left(\overrightarrow{I}\right)=\prod_{t=1}^{M}p(I_t)$ and $p(I_t)$ is $\sim$Bern (0.5).

Afterwards, the MCMC scheme [Liu, 2008] is applied to sample the posterior distribution $p(\overrightarrow{I}|\mathbf{X})$ of time points as being change points, with a randomly initial segment indicator vector $\overrightarrow{I}^0$. Details of the BCCPM algorithm are described in **Algorithm 1** as below.

The algorithm of Bayesian connectivity change point model

1. **Initialize** $\overrightarrow{I}$
   Initialize the initial segment indicator vector $\overrightarrow{I}^0$ randomly.
2. **Iterate *n* from 1 to a given number *N***
   1. Generate a new segment indicator vector by randomly choosing an indicator in and change its value from 0 to 1 or from 1 to 0.
   2. Calculate according to Eq. (6).
   3. Generate a random number u from uniform (0,1) and set

$$\overrightarrow{I}^n=\begin{cases}\overrightarrow{I}^* & \text{if}\quad u\le\min\left[1,\ \dfrac{p(\overrightarrow{I}^*|\mathbf{X})}{p(\overrightarrow{I}^{n-1}|\mathbf{X})}\right]\\ \overrightarrow{I}^{n-1} & \text{otherwise}\end{cases} \quad (7)$$

3. **Calculate** $p(\overrightarrow{I}|\mathbf{X})$
   1. Exclude the burn-in from the actual MCMC sample of the posterior distribution.
   2. Calculate the posterior probability for each time point to be a change point from MCMC samples.

Algorithm 1. The algorithm of BCCPM.

FIP Estimation and Vectorization

Given the change points detected via the BCCPM in section Bayesian connectivity change point model, the whole R-fMRI time series of each subject are divided into several segments, as shown in Figure 1b. Here, the pairwise functional interaction is defined as the absolute value of the Pearson correlations [Friston, 1994; Li et al., 2013a; Zhang et al., 2013b] between every pair of the R-fMRI time series segments separated by those change points, as follows:

$$\begin{aligned}R_{i,j,t}&=\text{abs}\left(\text{corr}\left(TS_{i,t},\ TS_{j,t}\right)\right),\ R_{i,j,t}=0,\ \textit{if}\ i=j;\\ \text{FIP}_t&=\left\{R_{i,j,t}|i,j\in(1,358)\right\}\end{aligned} \quad (8)$$

where FIP_t denotes the FIP within the t-th R-fMRI time series segment, which is a set of correlations from the congregation of all $R_{i,j,t}$ over each combination of i and j, and thus is a symmetrical connectivity matrix with the dimension of 358 $\times$ 358, $TS_{i,t}$ denotes the t-th R-fMRI time series segment between the t-th and $(t+1)$-th change points extracted from the i-th DICCCOL. Considering the symmetry of the FIP matrix, the upper triangular (excluding the zero diagonal) elements of the FIP matrix are concatenated to make a vector of $\boldsymbol{p}=(358\times357)/2=63903$ dimensions, denoted as FCV. Due to the intrinsically established correspondences of the DICCCOL landmarks across individual brains [Zhu et al., 2013], FCVs from different R-fMRI time series segments across different brains can be readily pooled and integrated to form a FCV matrix for further analysis as follows.

Atomic Functional Interaction Patterns Learning

Here, we premise that the whole-brain FIPs can be approximated by a linear combination of the AFIPs among brain networks. Based on the above method in Section FIP Estimation and Vectorization, the FIP matrices from different R-fMRI time series segments across different brains are vectorized and congregated into a single FCV matrix. To compute the AFIPs, a matrix factorization model is applied to the FCV matrix, as follows

$$\mathbf{V}\approx\mathbf{WH}, \quad (9)$$

where columns of $\mathbf{V}_{p\times q}$, that is, FCVs, are the FIP matrix representatives, and columns of $\mathbf{W}_{p\times r}$ are vectorized representatives of the AFIPs, that is, the upper triangular elements of the AFIP matrices. Here, p denotes the dimension of FCV, q denotes the number of FCVs, and r denotes the rank of $\mathbf{W}$, which is also the number of the AFIPs.

In this work, $\mathbf{H}$ is assumed to the projection of $\mathbf{V}$ onto $\mathbf{W}$, that is, $\mathbf{H}=\mathbf{W}^T\mathbf{V}$. With the nonnegative constraints on

the elements of **W** and **H**, our nonnegative AFIPs become the solution to the following optimization problem:

$$\begin{aligned}&\min_{\mathbf{W}\geq 0}||\mathbf{V}-\mathbf{W}\mathbf{W}^T\mathbf{V}|| \Longleftrightarrow \min_{\mathbf{W}\geq 0} D(\mathbf{V}\parallel\mathbf{U})\\ =&\min_{\mathbf{W}\geq 0}\sum_{i,j}\left(V_{i,j}\log\frac{V_{i,j}}{U_{i,j}}-V_{i,j}+U_{i,j}\right)(\mathbf{U}=\mathbf{W}\mathbf{W}^T\mathbf{V})\end{aligned} \tag{10}$$

where $||\cdot||$ is a matrix norm, and $D(\mathbf{V}\parallel\mathbf{U})$ is the matrix divergence of **V** from **U**, which can be viewed as a variant of the Kullback–Leibler divergence. Using the gradient descent approach, the above optimization function can be minimized by updating:

$$W_{i,j}\leftarrow W_{i,j}-\eta_{i,j}\frac{\partial D(\mathbf{V}\parallel\mathbf{W}\mathbf{W}^T\mathbf{V})}{\partial W_{i,j}}, \tag{11}$$

where $\eta_{i,j}$ is a nonnegative step size. For the divergence, the gradient in Eq. (11) is:

$$\begin{aligned}\frac{\partial D(\mathbf{V}\parallel\mathbf{W}\mathbf{W}^T\mathbf{V})}{\partial W_{i,j}}=&\sum_k\left((\mathbf{W}^T\mathbf{V})_{j,k}+\sum_l W_{l,j}V_{i,k}\right)-\\ &\sum_k\frac{V_{i,k}(\mathbf{W}^T\mathbf{V})_{j,k}}{(\mathbf{W}\mathbf{W}^T\mathbf{V})_{i,k}}-\sum_k V_{i,k}\sum_l\frac{W_{l,j}V_{l,k}}{(\mathbf{W}\mathbf{W}^T\mathbf{V})_{l,k}}\end{aligned}. \tag{12}$$

To keep the elements of **W** nonnegative, the step size in Eq. (11) is set as follows

$$\eta_{i,j}=\frac{W_{i,j}}{\sum_k((\mathbf{W}^T\mathbf{V})_{j,k}+\sum_l W_{l,j}V_{i,k})}. \tag{13}$$

Thus, the multiplicative updating rule is obtained as:

$$W_{i,j}\leftarrow W_{i,j}\frac{\sum_k V_{i,k}(\mathbf{W}^T\mathbf{V})_{j,k}/(\mathbf{W}\mathbf{W}^T\mathbf{V})_{i,k}+\sum_k V_{i,k}\sum_l W_{l,j}V_{l,k}/(\mathbf{W}\mathbf{W}^T\mathbf{V})_{l,k}}{\sum_k(\mathbf{W}^T\mathbf{V})_{j,k}+\sum_l W_{l,j}V_{i,k}}. \tag{14}$$

For stability of the convergence, **W** is normalized by 2-norm at each iteration.

Notably, a critical issue in matrix decomposition analysis is the selection of the number of factors, that is, the rank of **W**, r. Previous studies attempted to estimate the optimal rank r based on the cophenetic correlation coefficient [Brunet et al., 2004; Pascual-Montano et al., 2006] or a variant of the residual sum of squares of the approximated data matrix [Hutchins et al., 2008]. The basic ideal of rank selection based on the cophenetic correlation coefficient is that if a clustering of k classes is strong, the sample assignment to clusters would vary little from run to run [Brunet et al., 2004] (due to the random initializations, we cannot exactly obtain the same clustering results on each run). For each run, a clustering connectivity matrix $\mathbf{C}_{n\times n}$ (n is the number of samples) is defined to indicate the clustering results, in which entry $c_{i,j}=1$ if samples i and j belong the same cluster, otherwise $c_{i,j}=0$. Then a consensus matrix $\bar{\mathbf{C}}$, defined as the average clustering connectivity matrix over many runs, can be calculated. For a stable clustering algorithm, the entries of $\bar{\mathbf{C}}$ will be close to 0 or 1. Thus, the dispersion between 0 and 1 measures the reproducibility of the clustering algorithm with respect to random initializations. The cophenetic correlation coefficient is measured by the Pearson correlation of two distant matrices: the distance between samples induce by the consensus matrix, $\mathbf{I}-\bar{\mathbf{C}}$, and the distance between samples is induced by the linkage used in the reordering of $\bar{\mathbf{C}}$ [Brunet et al., 2004].

Notably, the optimization function for the transposed data matrix $\mathbf{V}^T$ in Eq. (10) is equivalent to the objective function of the k-means clustering under the assumption that the columns of **W** are orthonormal. Actually, the columns of **W** can be considered to be orthonormal [Yang et al., 2007]. Assume we want to cluster a dataset $\mathbf{V}=[v_1,v_2,\ldots,v_n]$ into k clusters C_1, C_2, …, C_k, whose centroids are O_1, O_2, …, O_k. The objective function of k-means clustering is [Ding et al., 2005]:

$$J_k=\sum_{j=1}^{k}\sum_{i\in C_i}||v_i-O_j||^2=\text{trace}\left[\mathbf{V}^T\mathbf{V}\right]-\text{trace}\left[\mathbf{A}^T\mathbf{V}^T\mathbf{V}\mathbf{A}\right], \tag{15}$$

where the element $a_{i,j}$ in the cluster indicator matrix $\mathbf{A}_{n\times k}$ is one if data vector v_i belongs to cluster C_j, zeros otherwise. Because each data vector belongs to one and only one cluster, columns of **A** are orthogonal. The optimization function in Eq. (10) for the transposed data matrix $\mathbf{V}^T$ is:

$$\begin{aligned}&||\mathbf{V}^T-\mathbf{W}\mathbf{W}^T\mathbf{V}^T||^2=\text{trace}\left[(\mathbf{V}^T-\mathbf{W}\mathbf{W}^T\mathbf{V}^T)(\mathbf{V}-\mathbf{V}\mathbf{W}\mathbf{W}^T)\right]\\ =&\text{trace}\left[\mathbf{V}^T\mathbf{V}\right]-2\text{trace}\left[\mathbf{W}^T\mathbf{V}^T\mathbf{V}\mathbf{W}\right]+\text{trace}\left[\mathbf{W}\mathbf{W}^T\mathbf{V}^T\mathbf{V}\mathbf{W}\mathbf{W}^T\right].\end{aligned} \tag{16}$$

The last term becomes $\text{trace}\left[\mathbf{W}^T\mathbf{V}^T\mathbf{W}\mathbf{V}\right]$ under the assumption that the columns of **W** are orthonormal, that is, $\mathbf{W}^T\mathbf{W}=\mathbf{I}$. If we choose the maximum element on each row as the cluster indicator, **W** becomes equivalent to the cluster indicator matrix **A** in k-means clustering. Due to the intrinsic relation between the DPNMF and the k-means clustering, and the random initialization of W in DPNMF, in this work, we adopted the cophenetic correlation

coefficient to determine the optimal rank r. The optimal value of r is where the magnitude of the cophenetic correlation coefficient falls. We experimentally found that 30–50 runs are sufficient for $\bar{\mathbf{C}}$ to be stable in our applications.

RESULTS

In this section, we applied the BCCPM described in Section Bayesian Connectivity Change Point Model to the R-fMRI time series of each subject for detecting change points in them (Section Change Points Detected by the BCCPM). After FIP estimation and vectorization, the DPNMF was applied to the derived FCV matrices for AFIPL (Section AFIPL on R-fMRI Datasets of ADHD and NC). Subsequently, the matrix divergences of the FCV matrix of each subject from its reconstructed FCV matrices based on the leant AFIPs from ADHD and NC, were calculated and compared for classification ADHD patients from NC subjects, respectively (Section Classification Analysis). The reproducibility of the learned AFIPs and their classification performance was assessed via a fivefold cross-validation strategy (Section Reproducibility Results). Finally, comparisons of AFIPL using the SNMF [Brunet et al., 2004; Lee and Seung, 1999] and the NPNMF (Section Comparisons with Other Nonnegative Matrix Factorization Method), as well as with the k-means algorithm, were provided (Section Comparisons with the k-Means Method).

Change Points Detected by the BCCPM

Based on the methods discussed in Section Bayesian Connectivity Change Point Model, the BCCPM was applied to the R-fMRI dataset of ADHD and NC subjects described in Section Data Acquisition and Preprocessing. For the sake of applicability and scalability, there are two important parameters in the BCCPM: one is prior information related to the change point number, denoted as, here

$$\rho=\log\frac{p(I_t=1)}{1-p(I_t=1)} \tag{17}$$

where $p(I_t=1)$ is the prior probability of the time point t being a change point. Normally, $p(I_t=1)$ is set as 0.5 by default which indicates that every time point has equal probability to be a change point and thus $\rho=0$. If it is desirable to detect more change points, bigger $p(I_t=1)$ should be chosen and thus positive value of ρ should be set. If less change points are desired, negative value of ρ is preferred. The other parameter is the initial segment indicator vector related to the change point locations, denoted as $\overrightarrow{I}^0$. If we do not know any prior information about the change point locations, the parameter $\overrightarrow{I}^0$ should be set as a randomly binary vector. However, if we know any possible change point location, it could be contained in the parameter $\overrightarrow{I}^0$, that is, the values in the binary vector corresponding to the change point locations could be set as 1. Given the R-fMRI time series, how many and where the change points would be detected are unknown. Thus, the parameter ρ is set as 0 and the parameter $\overrightarrow{I}^0$ is set as a randomly binary vector.

The segment indicator $\overrightarrow{I}$ of each subject obtained by the BCCPM was plotted with a randomly selected color, as shown in Figure 2. There are three time points with the posterior probability $\boldsymbol{p}(\boldsymbol{I}_t)=1$ in each line (the starting time point is always defined as a change point), that is, three change points were detected by the BCCPM for each subject. Then, the whole R-fMRI time series of each subject could be divided into three segments, each of which can be used to estimate a FIP.

AFIPL on R-fMRI Datasets of ADHD and NC

As mentioned above, three R-fMRI time series segments were obtained from the whole R-fMRI time series of each subject, and hence three FIPs could be constructed for each subject. Totally, there were 69 FCVs for the 23 ADHD patients and another 135 FCVs for the 45 NC subjects. Since the DICCCOL definition of ROIs provides us an inherently universal reference system across different brains, after vectorization, we congregated the FCVs to make three FCV matrices of ADHD ($\mathbf{V}^{\mathrm{ADHD}}_{63903\times69}$), NC ($\mathbf{V}^{\mathrm{NC}}_{63903\times135}$), and pooled ADHD and NC ($\mathbf{V}^{\mathrm{all}}_{63903\times204}$) (used for rank selection). First, the consensus matrices and the cophenetic correlation coefficients of the pooled ADHD and NC FCV matrix, $\mathbf{V}^{\mathrm{all}}_{63903\times204}$, were calculated using the above DPNMF and clustering methods, as described in Section Atomic Functional Interaction Patterns Learning. The results are shown in Figure 3. Figure 3a shows the consensus matrices generated for ranks r from 2 to 7. Although the cophenetic correlation coefficient falls at the ranks of 2, 3, 4, 6, 7, 9, it drops off more steeply at rank $r=2$ (Fig. 3b), and the consensus matrix at rank $r=2$ has the clearest block diagonal pattern (Fig. 3a), that is, the algorithm achieves the most robustness clustering results and is least sensitive to random initializations for $r=2$. Thus, the optimal rank is estimated as 2 in this work.

With the rank of 2, we applied the DPNMF to the two FCV matrices, $\mathbf{V}^{\mathrm{ADHD}}_{63903\times69}$ and $\mathbf{V}^{\mathrm{NC}}_{63903\times135}$, and four normalized representatives of AFIPs, that is, $\mathbf{W}^{\mathrm{ADHD}}_{63903\times2}$ and $\mathbf{W}^{\mathrm{NC}}_{63903\times2}$, were derived for ADHD and NC, as shown in Figure 4a. Then, we experimentally chose the top 400 high functional interaction pairs between DICCCOLs in each AFIP to be visualized on the three different views of cortical surfaces, as shown in Figures 4b–d. By comparing the common connections (edges) on the cortical surfaces between the four AFIPs, they could be categorized into two pairs: one common pair composed of ADHD-AFIP1 and NC-AFIP#1, where there are 310 common connections between them, and another distinctive pair composed of ADHD-AFIP#2 and NC-AFIP#2, where there are only 27 common connections between them. Therefore, the

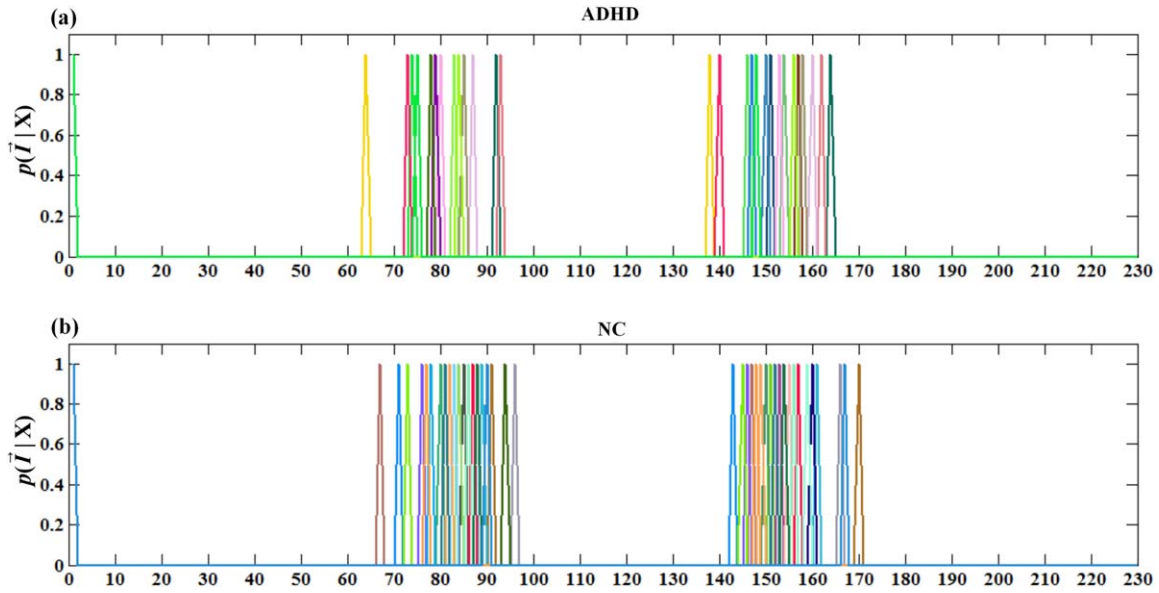

Figure 2.

The temporal distributions of the locations of change points detected by the BCCPM in the R-fMRI time series of each subject. The segment indicator vectors $\vec{I}$ of different subjects were plotted with different colors (randomly selected), in which one indicates that there is a change point at that time point. The first time point is always considered as a change point. The horizontal axis denotes the time points, and the vertical axis denotes the probability of each time point as being a change point. [Color figure can be viewed in the online issue, which is available at wileyonlinelibrary.com.]

common pair can be viewed as the common interaction patterns within subnetworks in both ADHD and NC, while the distinctive pair reflects the abnormal interaction patterns within subnetworks in ADHD. The neuroscience meanings of these four AFIPs are interpreted as follows. ADHD-AFIP#1 and NC-AFIP#1 both exhibit activities in the default mode networks (DMN) [Fox and Raichle, 2007; Raichle et al., 2001] as highlighted by the yellow circles in Figure 4, and also involves interhemisphere connections in the parietal lobe, occipital lobe, and the dorsal part of the visual cortex, as highlighted by the oval shapes. ADHD-AFIP#2 and NC-AFIP#2 involve strong connections between hemispheres in the parietal lobes and temporal lobes. Two clear differences between ADHD-AFIP#2 and NC-AFIP#2 are observed in Figure 4, as highlighted by the oval shape. The first difference is that ADHD-AFIP#2 exhibits strong interhemisphere connections in the prefrontal cortex, while NC-AFIP#2 shows few connections in the prefrontal cortex, which is in agreement with current knowledge about ADHD that ADHD reflects connectivity alternations in prefrontal-striatal circuitry [Castellanos and Proal, 2012]. The second difference is that NC-AFIP#2 exhibits much denser connections along the dorsal part of the posterior frontal lobes and anterior parietal lobes. The two different functional subnetworks between ADHD-AFIP#2 and NC-AFIP#2 indicate the abnormal FIPs in ADHD, and can be viewed as the AFSNs. According to the meta-analysis of functional roles of DICCCOLs [Yuan et al., 2013], the DICCCOLs (nodes of the subnetworks) involved in the two AFSNs are mainly related to the attention and working memory subnetworks, which is in agreement with current knowledge about the pathological origins of ADHD [e.g., Cortese, 2012; Krain and Castellanos, 2006]. To quantitatively elucidate the two AFSNs, we constructed two functional connectivity matrices for ADHD-AFIP#2 and NC-AFIP#2 as follows. Once the 400 high functional interaction pairs were chosen, their corresponding entries in the functional connectivity matrix are set to one, while the rest are set to zero. Then we accumulatively calculate the functional connectivity strength of each DICCCOL, as shown in Figure 5b. This result suggests that ADHD exhibit both increased and decreased FIPs, in comparison to NC. Interestingly, there are two major increased and decreased FIPs, which are consistent with the two AFSNs. Conceptually, that is one of the major methodological contribution of this work.

Besides, to further explore the neuroscience interpretation of the AFIPs in Figure 4, both less and more functional interaction pairs between DICCCOLs in each AFIP are visualized on the cortical surfaces, as shown in Supporting Information Figures 2 and 3. The visualizations in Supporting Information Figures 2 and 3 further confirm the above findings in Figure 4, where ADHD-AFIP#1 and NC-AFIP#1 construct the common pair, and ADHD-

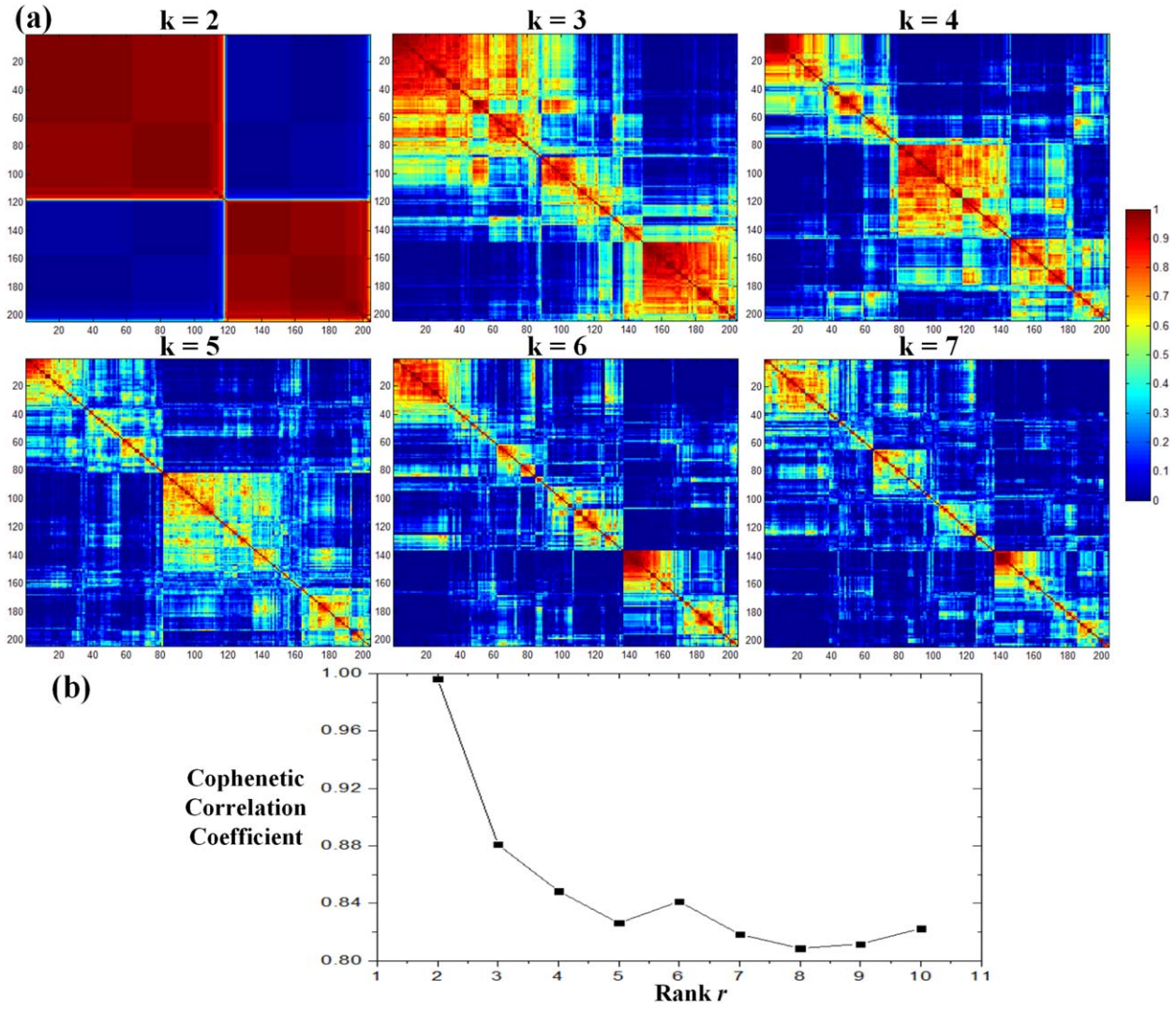

Figure 3.

(**a**) Reordered consensus matrices averaging 50 clustering connectivity matrices with rank r from 2 to 7. The clear block diagonal pattern at rank $r = 2$ indicates its robustness for clustering. (**b**) Cophenetic correlation coefficients for those consensus matrices in (a), with the steepest drop off at $r = 2$. [Color figure can be viewed in the online issue, which is available at wileyonlinelibrary.com.]

AFIP#2 and NC-AFIP#2 form the abnormal pair. Moreover, the two AFSNs are also observed in Supporting information Figures 2 and 3, as highlighted by the oval shapes, and even occur in the AFIPL using the SNMF and NPNMF approaches, as described later in Section Comparisons with Other Nonnegative Matrix Factorization Method. This is another major methodological contribution of this work.

Classification Analysis

As discussed in Section Change Points Detected by the BCCPM, we can construct a FCV matrix for subject s, that is, $\mathbf{V}^s_{63903\times 3}$, and reconstruct two FCV matrices, for example, $V^{s'} = \mathbf{W}\mathbf{W}^T V^s$, based on $\mathbf{W}^{\mathrm{ADHD}}_{63903\times 2}$ and $\mathbf{W}^{\mathrm{NC}}_{63903\times 2}$ respectively. Hence two matrix divergences, D_s^{ADHD} and D_s^{NC}, of the constructed FCV matrix V^s from its two reconstructed ones can be computed to evaluate the approximations to V^s based on Eq. (10). The matrix divergence is equivalent to the residual error of the approximation from the actual data. Thus, we can use the two matrix divergences of subject s for classification purpose based on the following criterions. If $D_s^{\mathrm{ADHD}} < D_s^{\mathrm{NC}}$, the subject s is classified as an ADHD patient, because the AFIPs derived from ADHD can better approximate the FIPs of the subject. On the contrary, if $D_s^{\mathrm{ADHD}} > D_s^{\mathrm{NC}}$, the subject s is classified as a NC subject. If

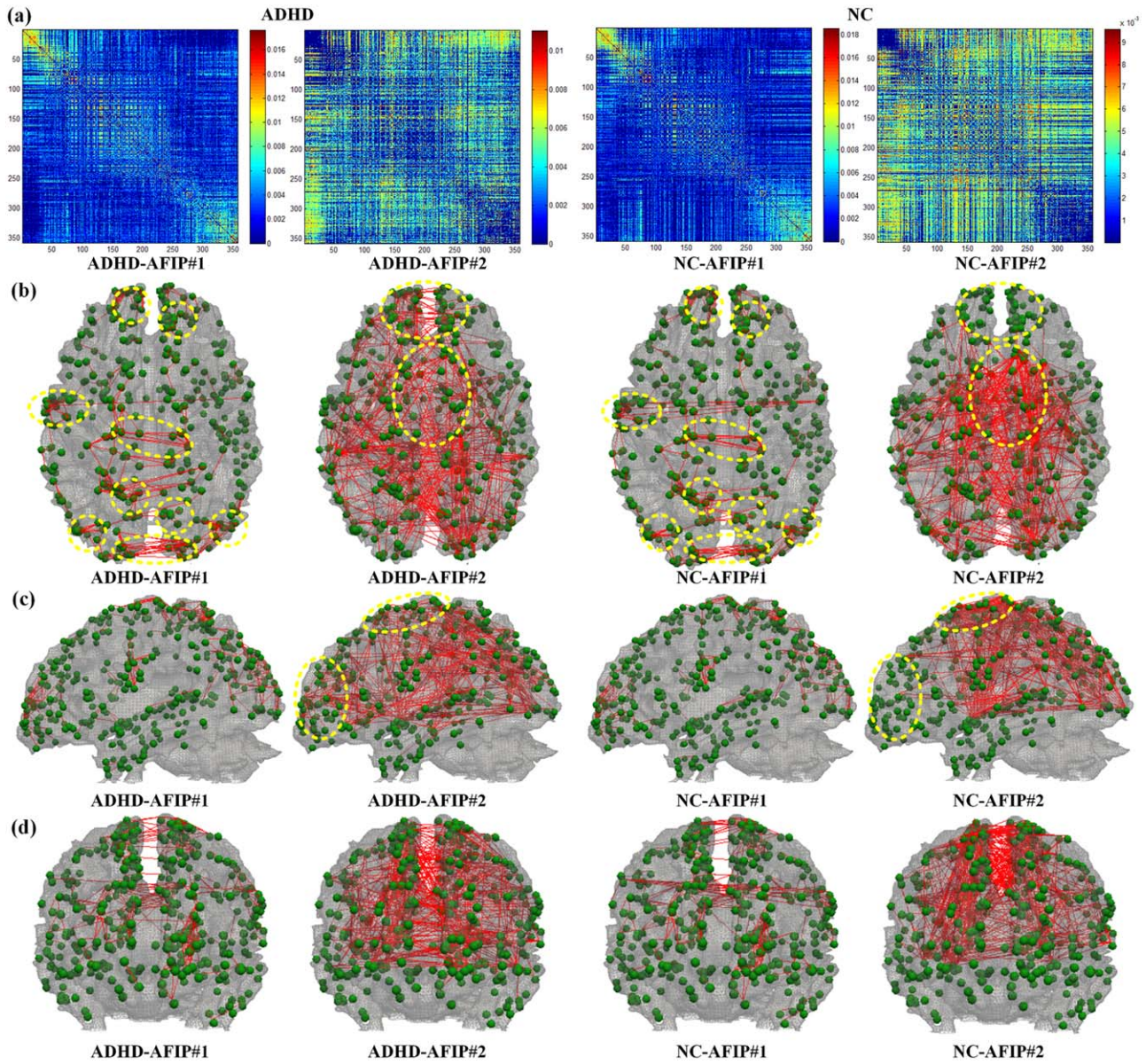

Figure 4.

(**a**) Visualization of the four AFIPs of ADHD and NC, whose vectorized representatives are columns of $\mathbf{W}^{\mathrm{ADHD}}_{63903\times 2}$ and $\mathbf{W}^{\mathrm{NC}}_{63903\times 2}$. (**b**)–(**d**) Visualization of the top 400 high functional interaction pairs between DICCCOLs in the four AFIPs on the three different views of cortical surfaces. The yellow circles in ADHD-AFIP1 and NC-AFIP#1 highlight the nodes involved in the DMN, and the oval shapes in ADHD-AFIP#2 and NC-AFIP#2 highlight the two AFSNs. DICCCOL ROIs are marked as green spheres on the cortical surfaces, and the functional interaction pairs between ROIs are shown as red edges connecting those spheres. [Color figure can be viewed in the online issue, which is available at wileyonlinelibrary.com.]

$D_s^{\mathrm{ADHD}} = D_s^{\mathrm{NC}}$, the subject s cannot be classified, which is very unlikely to happen actually, although it is possible theoretically. In our applications, we obtained $D_s^{\mathrm{ADHD}} \neq D_s^{\mathrm{NC}}$ for all subjects. The matrix divergences of all subjects are shown Figure 6. The blue bar indicates the matrix divergence of the FCV matrix $\mathbf{V}^s$ of each subject from its reconstructed one based on $\mathbf{W}^{\mathrm{NC}}_{63903\times 2}$. While the read bar indicates the matrix divergence of the FCV matrix $\mathbf{V}^s$ of each subject from the reconstructed one based on $\mathbf{W}^{\mathrm{ADHD}}_{63903\times 2}$. For all ADHD patients, we had $D_s^{\mathrm{ADHD}} < D_s^{\mathrm{NC}}$ (Fig. 6a), and for all NC subject we

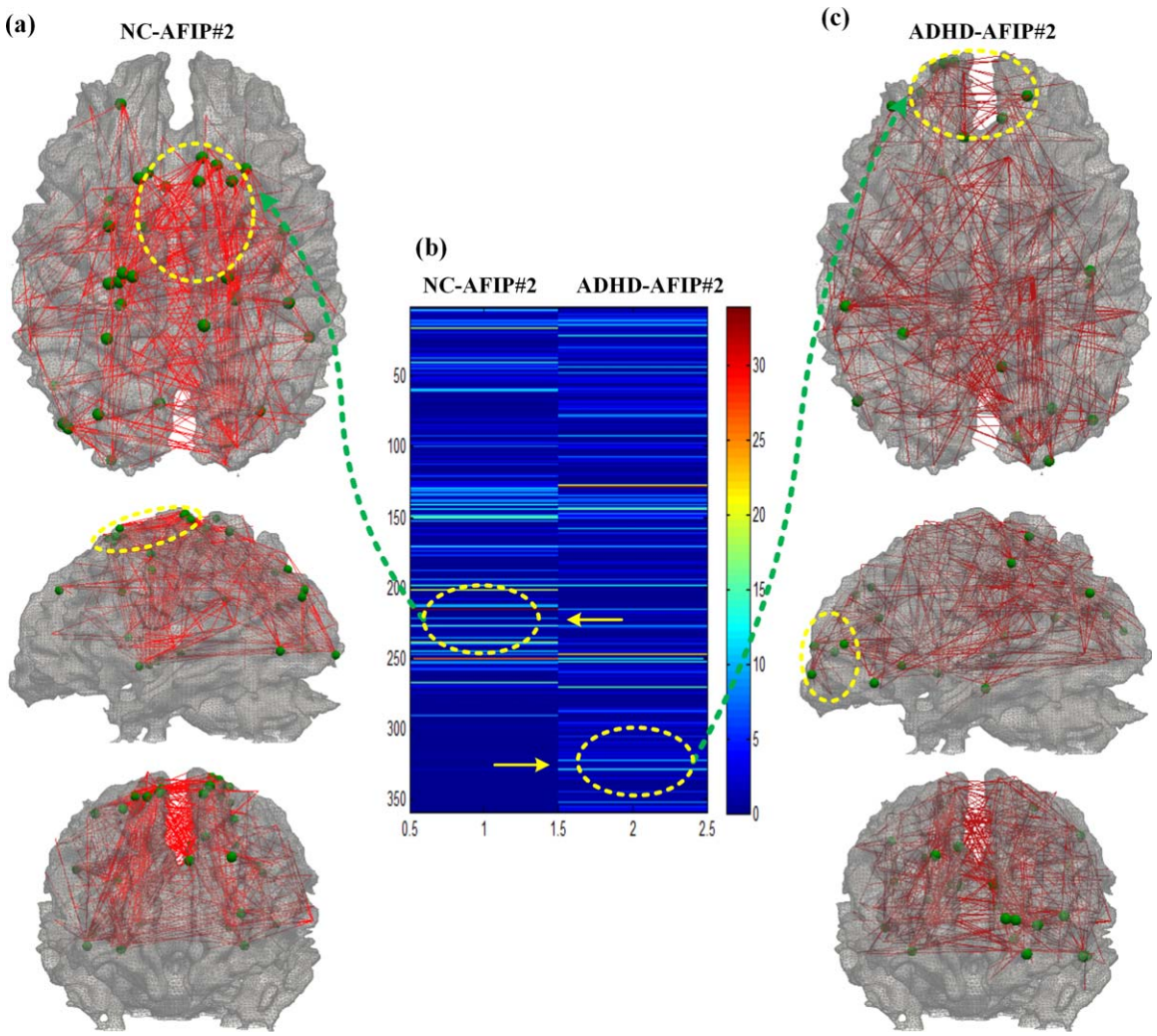

Figure 5.

The functional connectivity strengths of ADHD-AFIP#2 and NC-AFIP#2 are shown in (**b**). The DICCCOLs with decreased functional connectivity strength in ADHD are picked and visualized with the functional connectivities of NC-AFIP#2 for better illustration as shown in (**a**). The DICCCOLs with increased functional connectivity strength in ADHD are picked and visualized with the functional connectivities of ADHD-AFIP#2 for better illustration as shown in (**c**). The two decreased and increased FIPs are consistent with the two AFSNs, as highlighted by the oval shapes. [Color figure can be viewed in the online issue, which is available at wileyonlinelibrary.com.]

had $D_s^{\mathrm{ADHD}} > D_s^{\mathrm{NC}}$ (Fig. 6b), which means that we can successfully differentiate all ADHD patients from NC subjects without any false positive based on the above methods. This result suggests the effectiveness of the proposed computational pipeline.

Reproducibility Study

To examine the reproducibility of our AFIPL using the DPNMF, a fivefold cross-validation strategy was performed on the same dataset used in Section AFIPL on R-fMRI Datasets of ADHD and NC. The same dataset was divided into five portions, in which the first three portions consist of nine NC subjects and five ADHD patients, while the last two portions consist of nine NC subjects and four ADHD patients. The cross-validation training dataset was subsequently constructed by sequentially combining four portions into one, and the remaining portion was used as the testing dataset.

Then, AFIPL was performed on each of the fivefold training datasets with the same rank $r=2$ used in Section Classification Analysis. Four AFIPs were obtained from each training dataset, and also provided another

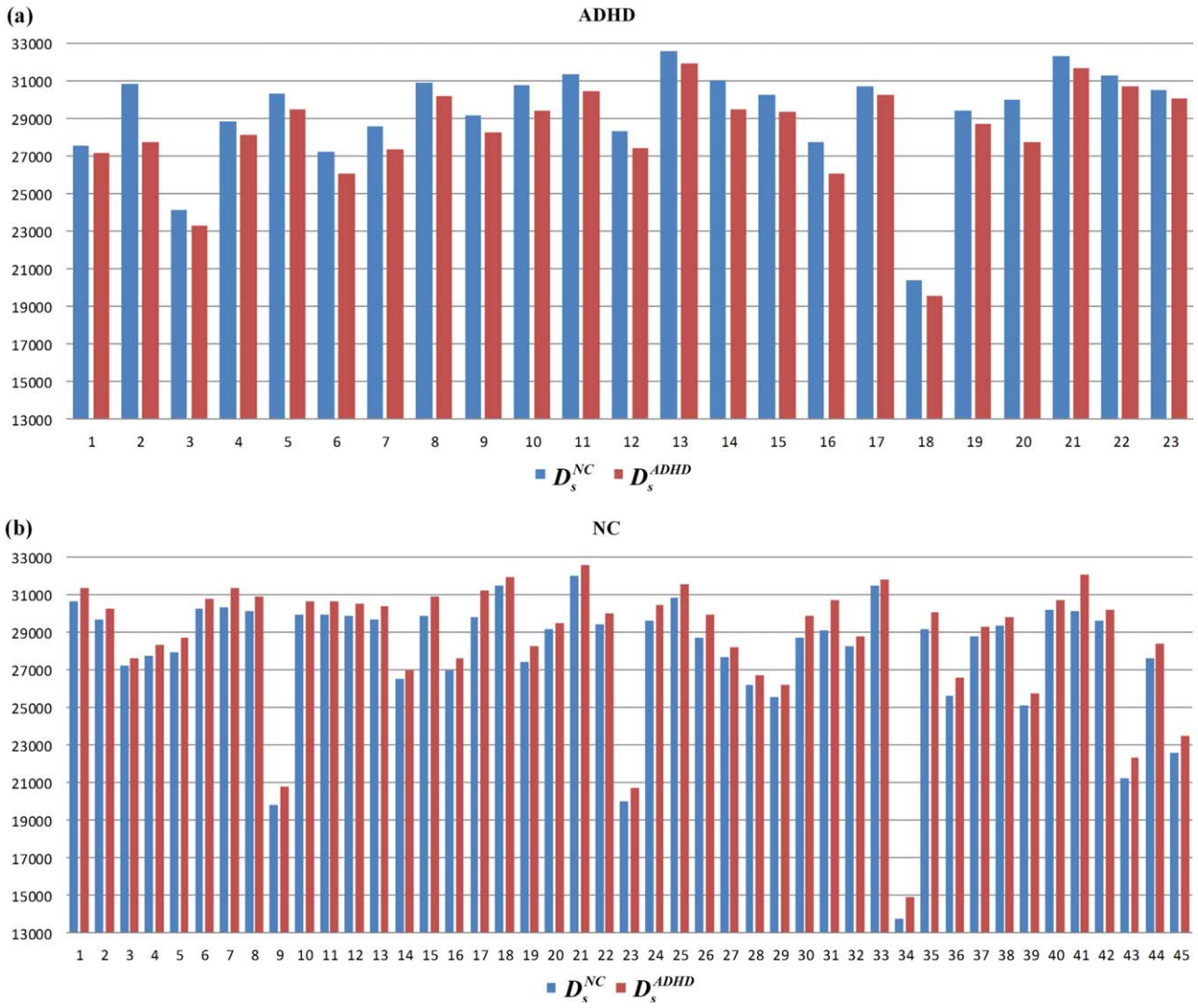

Figure 6.

The matrix divergence of the FCV matrix of each ADHD patient [panel (a)] and each NC subject [panel (b)] from its reconstructed FCV matrices based on $\mathbf{W}^{ADHD}_{63903\times2}$ and $\mathbf{W}^{NC}_{63903\times2}$. The blue bar indicates the matrix divergence of the FCV matrix from its reconstructed FCV matrix based on the AFIPs of NC, $\mathbf{W}^{NC}_{63903\times2}$. While the read bar indicates the matrix divergence of the FCV matrix from its reconstructed FCV matrix based on the AFIPs of ADHD, $\mathbf{W}^{ADHD}_{63903\times2}$. [Color figure can be viewed in the online issue, which is available at wileyonlinelibrary.com.]

supporting evidence to the observations in Figure 4, as shown in Supporting Information Figure 4. Notably, the four AFIPs can be reproduced across different folds with minor differences. These minor differences might be due to the differences in the training samples, which deserves further investigations using larger scale datasets in the future. The active areas involved in ADHD-AFIP#1 and NC-AFIP#1 were quite similar to the ones in Figure 4, and two AFSNs were also discovered in ADHD-AFIP#2 and NC-AFIP#2, which suggested the reproducibility of our findings discussed in Section AFIPL on R-fMRI Datasets of ADHD and NC.

Next, the same classification method described in Section Classification Analysis was applied on each of the fivefold testing datasets along with the AFIPs obtained from its corresponding training dataset. The classification results are provided in Table I and shown in Supporting Information Figure 5. On average, 92% of ADHD patients are successfully classified with only 5% false positive. The results demonstrated the efficiency and stability of the classification performance by our AFIPs.

TABLE I. List of the classification results of each of the five-fold testing datasets along with the AFIPs obtained from its corresponding training datasets

	Fold#1	Fold#2	Fold#3	Fold#4	Fold#5	Average
ADHD	5/5	4/5	4/5	4/4	4/4	92%
NC	8/9	8/9	9/9	9/9	9/9	95%

The entry of 4/5 in the table means that 4 subjects in the testing dataset consisting of five subjects are successfully classified.

Comparisons with Other NMF Method

To further demonstrate the effectiveness of our AFIPL using DPNMF, as described in Section Atomic Functional Interaction Patterns Learning, we also applied the SNMF method [Brunet et al., 2004; Lee and Seung, 1999] and the NPNMF method [Yang and Oja, 2010] on the same dataset. In the SNMF algorithm, to solve the approximation $\mathbf{V} \approx \mathbf{WH}$, matrices $\mathbf{W}$ and $\mathbf{H}$ are randomly initialized and iteratively updated to minimize the divergence function:

$$D(\mathbf{V} \parallel \mathbf{WH}) = \sum_{i,j} \left(V_{i,j} \log \frac{V_{i,j}}{(\mathbf{WH})_{i,j}} - V_{i,j} + (\mathbf{WH})_{i,j}\right). \quad (18)$$

At each iteration, $\mathbf{W}$ and $\mathbf{H}$ are updated as

$$H_{i,j} \leftarrow H_{i,j} \frac{\sum_k W_{k,i} V_{k,j}/(\mathbf{WH})_{k,j}}{\sum_k W_{k,i}}$$
$$W_{i,j} \leftarrow W_{i,j} \frac{\sum_k H_{j,k} V_{i,k}/(\mathbf{WH})_{i,k}}{\sum_k H_{j,k}}. \quad (19)$$

In the NPNMF algorithm, the optimization problem in Eq. (10) becomes:

$$\min_{\mathbf{W}\geq 0} ||\mathbf{V} - \mathbf{WW}^T\mathbf{V}|| \Longleftrightarrow \min_{\mathbf{W}\geq 0} ||\mathbf{V} - \mathbf{WW}^T\mathbf{V}||^2_{\text{Frobenius}}$$
$$= \min_{\mathbf{W}\geq 0} \text{trace}\left\{(\mathbf{V} - \mathbf{WW}^T\mathbf{V})(\mathbf{V} - \mathbf{WW}^T\mathbf{V})^T\right\} \quad (20)$$

and its corresponding multiplicative updating rule is:

$$W_{i,j} \leftarrow W_{i,j} \frac{2(\mathbf{VV}^T\mathbf{W})_{i,j}}{(\mathbf{WW}^T\mathbf{VV}^T\mathbf{W})_{i,j} + (\mathbf{VV}^T\mathbf{WW}^T\mathbf{W})_{i,j}}. \quad (21)$$

Subsequently, we performed AFIPL using SNMF and NPNMF on the same data used in Section AFIPL on R-fMRI Datasets of ADHD and NC. The consensus matrices and the cophenetic correlation coefficients of the FCV matrix of the pooled ADHD and NC, $\mathbf{V}^{\text{all}}_{63903\times 204}$, are shown in Figure 7. The consensus matrices shown in Figures 3 and 7 suggest that the AFIPL using DPNMF is more stable and less sensitive to random initializations than the ones using SNMF and NPNMF. The optimal rank for SNMF and NPNMF is still 2, as shown in Figure 7a,b. Moreover, we also evaluated the convergence of the consensus matrix derived from DPNMF, SNMF, and NPNMF, as shown in Supporting Information Figure 6. The AFIPL using DPNMF converge more quickly than using SNMF and NPNMF. The AFIPs derived via SNMF and NPNMF are visualized in Supporting Information Figures 7 and 8. Notably, the two AFSNs in ADHD-AFIP2 and NC-AFIP#2, which are observed in Figure 4, are also discovered in Supporting Information Figures 7 and 8, suggesting their robustness and reliability. The combination of ADHD-AFIP#1 and ADHD-AFIP#2 derived via SNMF (Supporting Information Figure 7) is similar to the combination of ADHD-AFIP#1 and ADHD-AFIP#2 derived via DPNMF (Figure 4) and NPNMF (Supporting Information Figure 8). It should be pointed out that the differences between the AFIPs derived via SNMF and DPNMF merit further analysis in the future. These comparison studies also provide another supporting evidence to the reproducibility of our AFIPs using DPNMF.

Comparisons with the k-Means Method

As discussed in Section Atomic Functional Interaction Patterns Learning, projective nonnegative matrix factorization (PNMF) has intrinsic relation to the k-means method. Thus, apart from the comparisons with SNMF and NPNMF, we also compared our AFIPL with the k-means method. Estimating the optimal cluster number is a crucial step in cluster analysis, and there are many validation methods [e.g., Fraley and Raftery, 2011; Halkidi et al., 2001], for instance, the Bayesian information criterion (BIC) [Schwarz, 1978], the entropy criterion [Celeux and Soromenho, 1996], and the gap statistic approach [Tibshirani et al., 2001]. The gap statistic approach is applicable to any clustering method, and does not require any prior knowledge on the model of the data. Notably, there is already an effective implementation of the gap statistic method as a the comprehensive R archive network (CRAN) package [Maechler et al., 2012]. Thus, to facilitate our study, we adopted the gap statistic method to estimate the optimal number of clusters. Suppose we cluster the data $\mathbf{V} = [v_1, v_2, \ldots, v_n]$ into k clusters $C_1, C_2, \ldots, C_k$. Let $d_{i,i'}$ denotes the distance between samples v_i and $v_{i'}$, the "gap" is defined as:

$$\mathbf{Gap}_n(k) = E^*_n\{\log(W_k)\} - \log(W_k)$$
$$W_k = \sum_{j=1}^{k} \frac{1}{2n_j} D_j, \qquad D_j = \sum_{i,i' \in C_j} d_{i,i'}, \quad (22)$$

where n_j is the number of samples in the cluster C_j, and E^*_n denotes expectation under a sample of size n from the reference distribution generated by Monte Carlo. The optimal number of clusters is estimated as the smallest k such that [Tibshirani et al., 2001]

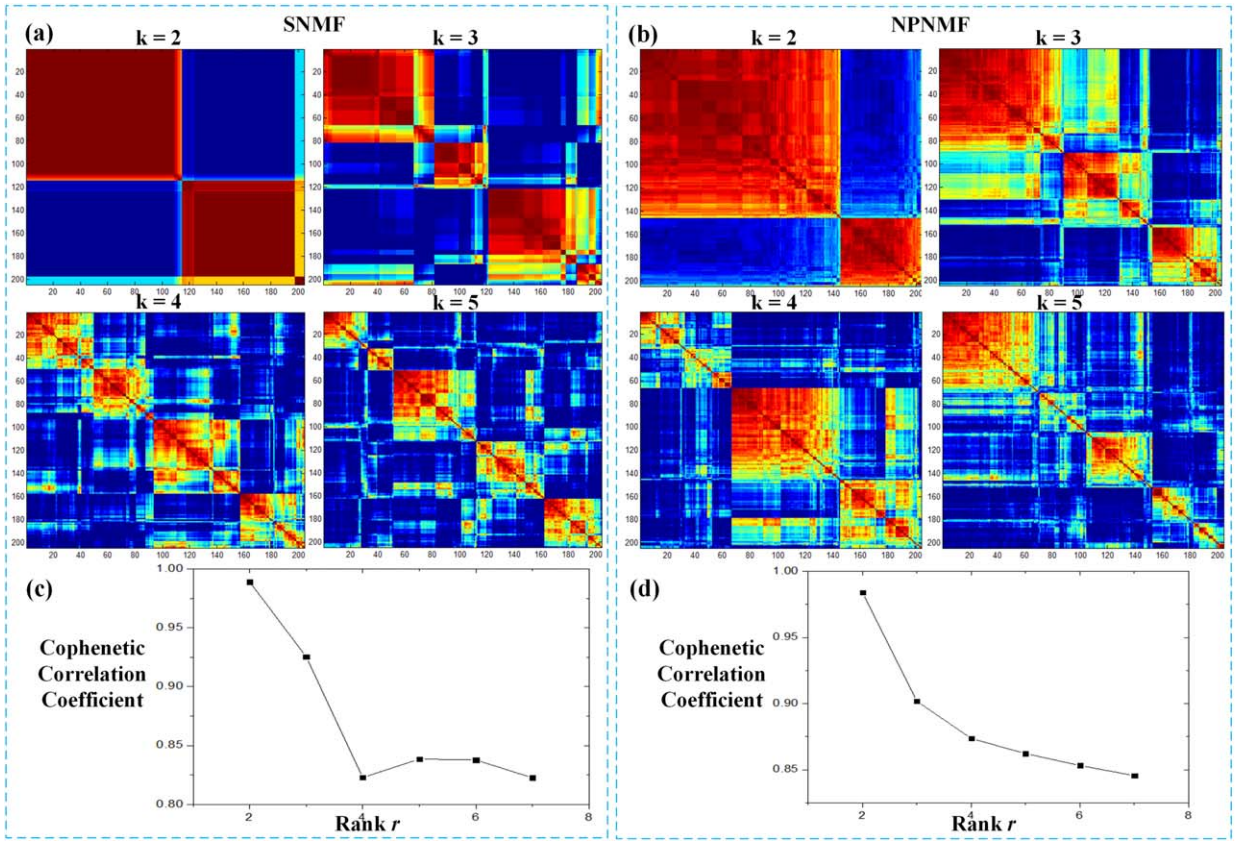

Figure 7.

Visualization of reordered consensus matrices averaging 50 clustering connectivity matrices with ranks *r* from 2 to 5 obtained via SNMF, (**a**), and NPNMF, (**b**). (**c**) The curve of cophenetic correlation coefficients for those consensus matrices in (*a*). (**d**) The curve of cophenetic correlation coefficients for those consensus matrices in (*b*). [Color figure can be viewed in the online issue, which is available at wileyonlinelibrary.com.]

$$\mathbf{Gap}(k) \geq \mathbf{Gap}(k+1) - s_{k+1} \tag{23}$$

The results of the gap statistic are shown in Supporting Information Figures 9a,b. The estimated number of clusters for ADHD patients is 2, while the one for NC is 3. For comparison purpose, we also tried to estimate the optimal number of clusters based on the BIC. A major difference between the gap statistic method and the BIC method is that the data v_i is assumed to come from the multivariate Gaussian mixture model in the BIC method. The optimal number of clusters is where the BIC reaches its maximum. As shown in Supporting Information Figures 9c,d, the estimated optimal number of clusters for ADHD patients is 2, while the one for NC is 3. This suggested the stability of the estimated optimal numbers of clusters. Then we applied the widely used *k*-means clustering algorithm to the FCV matrices of ADHD and NC with the estimated numbers of clusters, and the average of these FIPs which belong to the same cluster was calculated for each cluster. As before, the top 400 high functional interaction pairs between DICCCOLs in each averaged FIP are visualized on the cortical surfaces, as shown in Figure 8. Although the connectivity matrices of the averaged FIPs are remarkably different (the top panel in Fig. 8), the most connected DICCCOLs are quite similar (the bottom panel in Fig. 8). Our interpretation is that those averaged FIPs might be linearly related to each other to a certain degree. Interestingly, those most connected DICCCOLs in those averaged FIPs are quite similar to the ones in ADHD-AFIP#1 and NC-AFIP#1 (Fig. 4b). Thus, those FIPs can be characterized by ADHD-AFIP#1 or NC-AFIP#1 obtained from AFIPL using DPNMF. It also suggests that our AFIPL using DPNMF can reveal more meaningful phenomena which cannot be revealed by traditional clustering methods.

DISCUSSION AND CONCLUSIONS

In this work, we first applied the BCCPM to the R-fMRI time series to model functional interactions and their

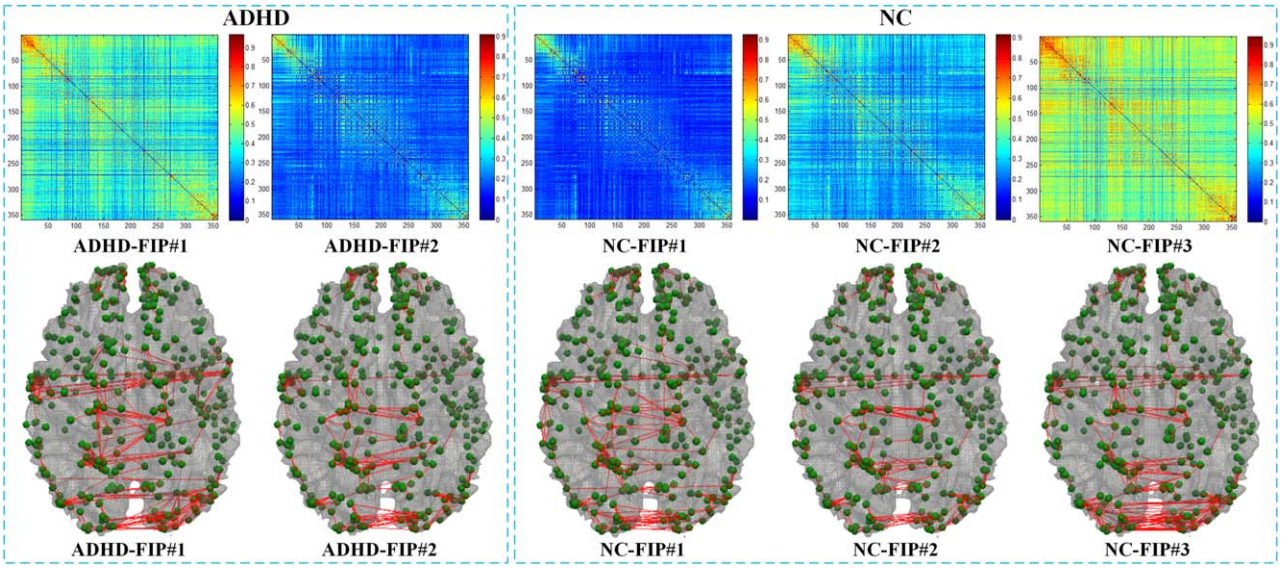

Figure 8.

Visualization of the averaged FIPs derived by *k*-means (top panel) and visualization of the top 400 high functional interaction pairs between DICCCOLs in each averaged FIP on the cortical surfaces (bottom panel). Although FIPs in top panel are remarkably different, their projections on the cortical surfaces are quite similar. [Color figure can be viewed in the online issue, which is available at wileyonlinelibrary.com.]

dynamics. FIPs were constructed via our recently developed 358 DICCCOLs [Zhu et al., 2013]. The optimal rank during DPNMF was determined by the cophenetic correlation coefficient [Brunet et al., 2004]. Then the DPNMF approaches were applied to the vectorized FIP matrices to learn the AFIPs in ADHD and NC. Four AFIPs were derived and can be grouped into two pairs, one common pair composed of ADHD-AFIP#1 and NC-AFIP#1, which suggested that NC brains and ADHD brains shared common AFIPs, and the other abnormal pair composed of ADHD-AFIP#2 and NC-AFIP#2, which indicated the abnormal AFIPs in ADHD brains. By further visualization analysis of the abnormal pair of ADHD-AFIP#2 and NC-AFIP#2, two AFSNs were discovered, which were reproduced during cross-validations and comparison studies with SNMF and NPNMF. The two AFSNs reflect the decreased and increased interaction patterns within subnetworks in ADHD and are mainly related to the attention and working memory subnetworks according to the meta-analysis of functional roles of DICCCOLs [Yuan et al., 2013], which is consistent with current knowledge about pathological origins of ADHD [e.g., Castellanos and Proal, 2012; Cortese, 2012; Krain and Castellanos, 2006].

In addition, the four AFIPs also have a good classification performance in differentiating ADHD patients from NC subjects. By comparing the matrix divergences of the FCV matrix of each subject from its reconstructed FCV matrices based the AFIPs of ADHD and NC, all the ADHD patients were successfully classified without any false positive. The fivefold cross validation confirmed the reproducibility of the meaningful biological phenomena and the good classification performance of the AFIPs.

In our study, we used the absolute value of the Pearson correlation between the R-fMRI time series of two ROIs to measure the coactivities between the two ROIs. Actually, the positive Pearson correlation measures the synchronous coactivities between two ROIs, while the negative one measures the asynchronous coactivities between two ROIs. In the network-level analysis of FIPs and AFIPs on the cortical surfaces, we aim to analyze both synchronous and asynchronous coactivities between ROIs simultaneously. Thus, we used the absolute values of the Pearson correlations for the FIP definition. In addition, the whole-brain network is functionally composed of many subnetworks, such as the default mode, working memory, and attention subnetworks. Due to the nonnegative constraints allowing only additive, not subtractive, combinations, NMF can effectively learn well part-based representations of a composite object [Lee and Seung, 1999; Yang et al., 2007]. Thus, we adopted an effective variant of NMF, that is, the DPNMF, to investigate the FIPs within subnetwork, that is, AFIPs, in this work.

Moreover, it should be noted that the connectivity matrices of the learnt AFIPs are not directly comparable. Because of the different reconstructive coefficients associated with the AFIPs during matrix decomposition, higher magnitude of an entry in an AFIP does not mean stronger coactivities between the corresponding ROIs, as compared with another entry in another AFIP. However, the entries

in the same AFIP are still comparable. Hence we experimentally chose the top 400 high interaction pairs in the AFIPs, other than a global threshold, to be visualized on the cortical surfaces for network-level analysis and comparison. The comparisons between the AFIPs are based on their projections on the cortical surfaces.

A potential limitation of our work is that the BCCPM is not sensitive to small local structure changes within a small part of ROIs. In our study, we assume that the change points exist in all the ROIs. Thus, the BCCPM focuses on detecting the global change of network structure. However, if different ROIs have different change points for the same subject, the BCCPM would only detect the change points where most of the ROIs are involved in the change of structure.

In summary, our work contributed a novel computational framework for characterization and differentiation of ADHD and our experimental results have revealed novel insights about the abnormal functional interactions and dynamics in ADHD. In the future, this computational framework could be possibly applied in many other psychiatric disorders to elucidate the potentially abnormal brain functions in such brain conditions. Also, more indepth analyses of the neuroscientific meanings of the AFSNs, for example, those in the ADHD in Figure 4, should be performed by considering clinical and behavior datasets in the future.

ACKNOWLEDGMENT

The authors would like to thank the anonymous reviewers for their constructive comments.

REFERENCES

Allen EA, Damaraju E, Plis SM, Erhardt EB, Eichele T, Calhoun VD. (2012): Tracking whole-brain connectivity dynamics in the resting state. Cerebral cortex (in press).

Bassett DS, Wymbs NF, Porter MA, Mucha PJ, Carlson JM, Grafton ST. (2011): Dynamic reconfiguration of human brain networks during learning. Proc Natl Acad Sci USA 108:7641–7646.

Brunet J-P, Tamayo P, Golub TR, Mesirov JP. (2004): Metagenes and molecular pattern discovery using matrix factorization. Proc Natl Acad Sci 101:4164–4169.

Castellanos FX, Proal E. (2012): Large-scale brain systems in ADHD: Beyond the prefrontal-striatal model. Trends Cogn Sci 16:17–26.

Celeux G, Soromenho G. (1996): An entropy criterion for assessing the number of clusters in a mixture model. J Classification. 13: 195–212.

Chang C, Glover GH. (2010): Time-frequency dynamics of resting-state brain connectivity measured with fMRI. NeuroImage 50: 81–98.

Cortese S. (2012): The neurobiology and genetics of Attention-Deficit/Hyperactivity Disorder (ADHD): What every clinician should know. Eur J Paediatr Neurol 16:422–433.

Derrfuss J, Mar RA. (2009): Lost in localization: The need for a universal coordinate database. NeuroImage 48:1–7.

Ding C, He X, Simon HD. (2005): On the Equivalence of Nonnegative Matrix Factorization and Spectral Clustering. Proceedings of the 2005 SIAM International Conference on Data Mining. pp 606–610.

Fox MD, Raichle ME. (2007): Spontaneous fluctuations in brain activity observed with functional magnetic resonance imaging. Nat Rev Neurosci 8:700–711.

Fraley C, Raftery AE. (2011): Model-based clustering, discriminant analysis, and density estimation. J Am Stat Assoc 97:611–631.

Friston KJ. (1994): Functional and effective connectivity in neuroimaging: A synthesis. Hum Brain Mapping 2:56–78.

Gelman A, Carlin JB, Stern HS, Donald BR. (2003): Bayesian Data Analysis: Chapman & Hall/CRC Texts in Statistical Science. London: CRC press.

Ghanbari Y, Smith A, Schultz R, Verma R. (2013): Connectivity subnetwork learning for pathology and developmental variations. In: Mori K, Sakuma I, Sato Y, Barillot C, Navab N, editors. MICCAI, Berlin Heidelberg: Springer. pp 90–97.

Gilbert CD, Sigman M. (2007): Brain states: Top-down influences in sensory processing. Neuron 54:677–696.

Halkidi M, Batistakis Y, Vazirgiannis M. (2001): On clustering validation techniques. Journal of Intell Inf Syst 17:107–145.

Hutchins LN, Murphy SM, Singh P, Graber JH. (2008): Position-dependent motif characterization using non-negative matrix factorization. Bioinformatics 24:2684–2690.

Kaufman J, Birmaher B, Brent D, Rao U, Flynn C, Moreci P, Williamson D, Ryan N. (1997): Schedule for affective disorders and schizophrenia for school-age children-present and lifetime version (K-SADS-PL): Initial reliability and validity data. J Am Acad Child Adolesc Psychiatry 36:980–988.

Kim H, Park H. (2007): Sparse non-negative matrix factorizations via alternating non-negativity-constrained least squares for microarray data analysis. Bioinformatics 23:1495–1502.

Krain AL, Castellanos FX.. (2006): Brain development and ADHD. Clin Psychol Rev 26:433–444.

Lee DD, Seung HS. (1999): Learning the parts of objects by non-negative matrix factorization. Nature 401:788–791.

Li T, Ding C. (2006): The Relationships Among Various Nonnegative Matrix Factorization Methods for Clustering; 18-22 Dec. 2006; Data Mining, Sixth International Conference on Hongkong, ICDM '06. pp. 362–371.

Li X, Zhu D, Jiang X, Jin C, Zhang X, Guo L, Zhang J, Hu X, Li L, Liu T. (2013a): Dynamic functional connectomics signatures for characterization and differentiation of PTSD patients. Hum Brain Mapp 35:1761–1778.

Li X, Lim C, Li K, Guo L, Liu T. (2013b): Detecting brain state changes via fiber-centered functional connectivity analysis. Neuroinformatics 11:193–210.

Lian Z, Li X, Xing J, Lv J, Jiang X, Zhu D, Xu J, Potenza MN, Liu T, Zhang J : Exploring functional brain dynamics via a bayesian connectivity change point model; IEEE 11th International Symposium on Biomedical Imaging (ISBI), (in press).

Lindquist MA, Waugh C, Wager TD. (2007): Modeling state-related fMRI activity using change-point theory. NeuroImage 35:1125–1141.

Liu JS. (2008): Monte Carlo Strategies in Scientific Computing: Berlin: Springer-Verlag.

Liu T. (2011): A few thoughts on brain ROIs. Brain Imaging Behav 5:189–202.

Lynall ME, Bassett DS, Kerwin R, McKenna PJ, Kitzbichler M, Muller U, Bullmore E. (2010): Functional connectivity and brain networks in schizophrenia. J Neurosci 30:9477–9487.

Maechler M, Rousseeuw P, Struyf A, Hubert M, Hornik K. (2012). Cluster: Cluster Analysis Basics and Extensions. R package version. 1(2).

Majeed W, Magnuson M, Hasenkamp W, Schwarb H, Schumacher EH, Barsalou L, Keilholz SD. (2011): Spatiotemporal dynamics of low frequency BOLD fluctuations in rats and humans. NeuroImage 54:1140–1150.

Pascual-Montano A, Carmona-Saez P, Chagoyen M, Tirado F, Carazo JM, Pascual-Marqui RD. (2006): bioNMF: A versatile tool for non-negative matrix factorization in biology. BMC Bioinformatics 7:366.

Passingham RE, Stephan KE, Kotter R. (2002): The anatomical basis of functional localization in the cortex. Nat Rev Neurosci 3:606–616.

Poldrack RA. (2012): The future of fMRI in cognitive neuroscience. NeuroImage 62:1216–1220.

Qi Q, Zhao Y, Li M, Simon R. (2009): Non-negative matrix factorization of gene expression profiles: A plug-in for BRB-ArrayTools. Bioinformatics 25:545–547.

Raichle ME, MacLeod AM, Snyder AZ, Powers WJ, Gusnard DA, Shulman GL. (2001): A default mode of brain function. Proc Natl Acad Sci USA 98:676–682.

Robinson LF, Wager TD, Lindquist MA. (2010): Change point estimation in multi-subject fMRI studies. NeuroImage 49:1581–1592.

Schwarz G. (1978): Estimating the dimension of a model. Ann Stat 6:461–464.

Smith SM, Miller KL, Moeller S, Xu J, Auerbach EJ, Woolrich MW, Beckmann CF, Jenkinson M, Andersson J, Glasser MF, Van Essen DC, Feinberg DA, Yacoub ES, Ugurbil K. (2012): Temporally-independent functional modes of spontaneous brain activity. Proc Natl Acad Sci USA 109:3131–3136.

Tibshirani R, Walther G, Hastie T. (2001): Estimating the number of data clusters via the gap statistic. J R Statistical Soc B 63:411–423.

Trefethen LN, Bau III D. (1997). Numerical Linear Algebra: Philadelphia: SIAM.

Yang Z, Oja E. (2010): Linear and nonlinear projective nonnegative matrix factorization. IEEE Trans Neural Netw 21:734–749.

Yang Z, Yuan Z, Laaksonen J. (2007): Projective non-negative matrix factorization with applications to facial image processing. Int J Pattern Recognit Artif Intell 21:1353–1362.

Yuan Y, Jiang X, Zhu D, Chen H, Li K, Lv P, Yu X, Li X, Zhang S, Zhang T, Hu X, Han J, Guo L, Liu T. (2013): Meta-analysis of functional roles of DICCCOLs. Neuroinformatics 11:47–63.

Zhang X, Guo L, Li X, Zhu D, Li K, Sun Z, Jin C, Hu X, Han J, Zhao Q, Li L, Liu T. (2012). Characterization of task-free/task-performance brain states. In: Ayache N, Delingette H, Golland P, Mori K, editors. Medical Image Computing and Computer-Assisted Intervention – MICCAI. pp 237–245. Berlin, Heidelberg: Springer.

Zhang J, Li X, Li C, Lian Z, Huang X, Zhong G, Zhu D, Li K, Jin C, Hu X, Han J, Guo L, Hu X, Li L, Liu T. (2013a): Inferring functional interaction and transition patterns via dynamic bayesian variable partition models. Hum Brain Mapp (in press).

Zhang X, Guo L, Li X, Zhang T, Zhu D, Li K, Chen H, Lv J, Jin C, Zhao Q, Li L, Liu T. (2013b): Characterization of task-free and task-performance brain states via functional connectome patterns. Med Image Anal 17:1106–1122.

Zhu D, Li K, Faraco CC, Deng F, Zhang D, Guo L, Miller LS, Liu T. (2012): Optimization of functional brain ROIs via maximization of consistency of structural connectivity profiles. NeuroImage 59:1382–1393.

Zhu D, Li K, Guo L, Jiang X, Zhang T, Zhang D, Chen H, Deng F, Faraco C, Jin C, Wee C-Y, Yuan Y, Lv P, Yin Y, Hu X, Duan L, Hu X, Han J, Wang L, Shen D, Miller LS, Li L, Liu T. (2013): DICCCOL: dense individualized and common connectivity-based cortical landmarks. Cerebral Cortex 23:786–800.